Enhancement of two-photon photoluminescence and SERS for low-coverage gold films

SERGEY M. NOVIKOV,[1,*] JONAS BEERMANN,[1] CHRISTIAN FRYDENDAHL,[2] NICOLAS STENGER,[2] VICTOR COELLO,[3] N. ASGER MORTENSEN,[2] AND SERGEY I. BOZHEVOLNYI[1]

[1]Centre for Nano Optics, University of Southern Denmark, Campusvej 55, DK-5230 Odense, Denmark
[2]Department of Photonics Engineering, Technical University of Denmark, Ørsteds Plads 343, DK-2800 Kgs. Lyngby, Denmark
[3]CICESE Monterrey, Alianza Centro No.504 PIIT Apodaca, N. L. C. P. 66600, Mexico
*smn@iti.sdu.dk

Abstract: Electromagnetic field enhancement (FE) effects occurring in thin gold films 3-12-nm are investigated with two-photon photoluminescence (TPL) and Raman scanning optical microscopies. The samples are characterized using scanning electron microscopy images and linear optical spectroscopy. TPL images exhibit a strong increase in the level of TPL signals for films thicknesses 3–8-nm, near the percolation threshold. For some thicknesses, TPL measurements reveal super-cubic dependences on the incident power. We ascribe this feature to the occurrence of very strongly localized and enhanced electromagnetic fields due to multiple light scattering in random nanostructures that might eventually lead to white-light generation. Raman images exhibit increasing Raman signals when decreasing the film thickness from 12 to 6-nm and decreasing signal for the 3-nm-film. This feature correlates with the TPL observations indicating that highest FE is to be expected near the percolation threshold.

References and links

1. D. K. Gramotnev and S. I. Bozhevolnyi, "Plasmonics beyond the diffraction limit," Nat. Photonics **4**(2), 83–91 (2010).
2. J. A. Schuller, E. S. Barnard, W. Cai, Y. C. Jun, J. S. White, and M. L. Brongersma, "Plasmonics for extreme light concentration and manipulation," Nat. Mater. **9**(3), 193–204 (2010).
3. S. Maier, *Plasmonics: Fundamentals and Applications* (Springer, 2007).
4. S. Link, S. Lal, and N. J. Halas, "Plasmonics: nanoscale optics from sensing to waveguiding," Nat. Photonics **1**(11), 641–648 (2007).
5. J. N. Anker, W. P. Hall, O. Lyandres, N. C. Shah, J. Zhao, and R. P. Van Duyne, "Biosensing with plasmonic nanosensors," Nat. Mater. **7**(6), 442–453 (2008).
6. E. Ringe, M. R. Langille, K. Sohn, J. Zhang, J. Huang, C. A. Mirkin, R. P. Van Duyne, and L. D. Marks, "Plasmon length: an universal parameter to describe the size effects in gold nanoparticles," J. Phys. Chem. Lett. **3**(11), 1479–1483 (2012).
7. K. M. Mayer and J. H. Hafner, "Localized surface plasmon resonance sensors," Chem. Rev. **111**(6), 3828–3857 (2011).
8. F. L. Yap, P. Thoniyot, S. Krishnan, and S. Krishnamoorthy, "Nanoparticle cluster arrays for high-performance SERS through directed self-assembly on flat substrates and on optical fibers," ACS Nano **6**(3), 2056–2070 (2012).
9. J. Beermann, S. M. Novikov, O. Albrektsen, M. G. Nielsen, and S. I. Bozhevolnyi, "Surface-enhanced Raman imaging of fractal shaped periodic metal nanostructures," J. Opt. Soc. Am. B **26**(12), 2370 (2009).
10. J. Beermann, S. M. Novikov, K. Leosson, and S. I. Bozhevolnyi, "Surface enhanced Raman microscopy with metal nanoparticle arrays," J. Opt. A, Pure Appl. Opt. **11**(7), 075004 (2009).
11. A. K. Sarychev and V. M. Shalaev, "Electromagnetic field fluctuations and optical nonlinearities in metal-dielectric composites," Phys. Rep. **335**(6), 275–371 (2000).
12. L. Rodríguez-Lorenzo, J. M. Romo-Herrera, J. Pérez-Juste, R. A. Alvarez-Puebla, and L. M. Liz-Marzán, "Reshaping and LSPR tuning of Au nanostars in presence of CTAB," J. Mater. Chem. **21**(31), 11544–11549 (2011).
13. I. P. Radko, V. S. Volkov, J. Beermann, A. B. Evlyukhin, T. Søndergaard, A. Boltasseva, and S. I. Bozhevolnyi, "Plasmonic metasurfaces for waveguiding and field enhancement," Laser Photonics Rev. **3**(6), 575–590 (2009).

14. T. W. H. Oates, H. Sugime, and S. Noda, "Combinatorial Surface-Enhanced Raman Spectroscopy and Spectroscopic Ellipsometry of Silver Island Films," J. Phys. Chem. C **113**(12), 4820–4828 (2009).
15. D. Cialla, A. März, R. Böhme, F. Theil, K. Weber, M. Schmitt, and J. Popp, "Surface-enhanced Raman spectroscopy (SERS): progress and trends," Anal. Bioanal. Chem. **403**(1), 27–54 (2012).
16. A. Balčytis, T. Tolenis, X. Wang, G. Seniutinas, R. Drazdys, P. R. Stoddart, and S. Juodkazis, "Percolation threshold gold films on columnar coatings: characterisation for SERS applications," http://www arXiv:1603.08197.
17. S. Nie and S. R. Emory, "Probing single molecules and single nanoparticles by surface-enhanced Raman scattering," Science **275**(5303), 1102–1106 (1997).
18. K. Kneipp, Y. Wang, H. Kneipp, L. T. Perelman, I. Itzkan, R. R. Dasari, and M. S. Feld, "Single molecule detection using surface-enhanced Raman scattering (SERS)," Phys. Rev. Lett. **78**(9), 1667–1670 (1997).
19. A. Shiohara, Y. Wang, and L. M. Liz-Marzán, "Recent approaches toward creation of hot spots for SERS detection," J. Photochem. Photobiol. Chem. **21**, 2–25 (2014).
20. J. P. Camden, J. A. Dieringer, Y. Wang, D. J. Masiello, L. D. Marks, G. C. Schatz, and R. P. Van Duyne, "Probing the Structure of Single-Molecule Surface-Enhanced Raman Scattering Hot Spots," J. Am. Chem. Soc. **130**(38), 12616–12617 (2008).
21. M. Moskovits, "Imaging: Spot the hotspot," Nature **469**(7330), 307–308 (2011).
22. K. Ueno, S. Juodkazis, V. Mizeikis, K. Sasaki, and H. Misawa, "Clusters of Closely Spaced Gold Nanoparticles as a Source of Two-Photon photoluminescence at Visible Wavelengths," Adv. Mater. **20**(1), 26–30 (2008).
23. G. Toscano, S. Raza, A.-P. Jauho, N. A. Mortensen, and M. Wubs, "Modified field enhancement and extinction by plasmonic nanowire dimers due to nonlocal response," Opt. Express **20**(4), 4176–4188 (2012).
24. N. A. Mortensen, S. Raza, M. Wubs, T. Søndergaard, and S. I. Bozhevolnyi, "A generalized non-local optical response theory for plasmonic nanostructures," Nat. Commun. **5**, 3809 (2014).
25. N. Gandra, A. Abbas, L. Tian, and S. Singamaneni, "Plasmonic Planet-Satellite Analogues: Hierarchical Self-Assembly of Gold Nanostructures," Nano Lett. **12**(5), 2645–2651 (2012).
26. A. Shiohara, S. M. Novikov, D. M. Solís, J. M. Taboada, F. Obelleiro, and L. M. Liz-Marzán, "Plasmon Modes and Hot Spots in Gold Nanostar–Satellite Clusters," J. Phys. Chem. C **119**(20), 10836–10843 (2015).
27. M. Gaio, M. Castro-Lopez, J. Renger, N. van Hulst, and R. Sapienza, "Percolating plasmonic networks for light emission control," Faraday Discuss. **178**, 237–252 (2015).
28. S. Ducourtieux, V. A. Podolskiy, S. Gre'sillon, S. Buil, B. Berini, P. Gadenne, A. C. Boccara, J. C. Rivoal, W. D. Bragg, K. Banerjee, V. P. Safonov, V. P. Drachev, Z. C. Ying, A. K. Sarychev, and V. M. Shalaev, "Near-field optical studies of semicontinuous metal films," Phys. Rev. B **64**(16), 165403 (2001).
29. K. Seal, D. A. Genov, A. K. Sarychev, H. Noh, V. M. Shalaev, Z. C. Ying, X. Zhang, and H. Cao, "Coexistence of Localized and Delocalized Surface Plasmon Modes in Percolating Metal Films," Phys. Rev. Lett. **97**(20), 206103 (2006).
30. S. M. Novikov, A. B. Evlyukhin, A. I. Kuznetsov, J. Beermann, B. N. Chichkov, and S. I. Bozhevolnyi, "Characterization of localized field enhancements in laser fabricated gold needle nanostructures," J. Opt. Soc. Am. B **29**(1), 185–190 (2012).
31. A. Mooradian, "Photoluminescence of metals," Phys. Rev. Lett. **22**(5), 185–187 (1969).
32. G. T. Boyd, Z. H. Yu, and Y. R. Shen, "Photoinduced luminescence from the noble metals and its enhancement on roughened surfaces," Phys. Rev. B Condens. Matter **33**(12), 7923–7936 (1986).
33. J. Beermann, S. M. Novikov, T. Søndergaard, A. Boltasseva, and S. I. Bozhevolnyi, "Two-photon mapping of localized field enhancements in thin nanostrip antennas," Opt. Express **16**(22), 17302–17309 (2008).
34. S. D. Zuani, T. Peterseim, A. Berrier, B. Gompf, and M. Dressel, "Second harmonic generation enhancement at the percolation threshold," Appl. Phys. Lett. **104**(24), 241109 (2014).
35. P. Mühlschlegel, H.-J. Eisler, O. J. F. Martin, B. Hecht, and D. W. Pohl, "Resonant Optical Antennas," Science **308**(5728), 1607–1609 (2005).
36. M. Eichelbaum, B. E. Schmidt, H. Ibrahim, and K. Rademann, "Three-photon-induced luminescence of gold nanoparticles embedded in and located on the surface of glassy nanolayers," Nanotechnology **18**(35), 355702 (2007).
37. S. Raza, S. I. Bozhevolnyi, M. Wubs, and N. Asger Mortensen, "Nonlocal optical response in metallic nanostructures," J. Phys. Condens. Matter **27**(18), 183204 (2015).
38. A. V. Krasavin, P. Ginzburg, G. A. Wurtz, and A. V. Zayats, "Nonlocality-driven supercontinuum white light generation in plasmonic nanostructures," Nat. Commun. **7**, 11497 (2016).
39. P. J. Schuck, D. P. Fromm, A. Sundaramurthy, G. S. Kino, and W. E. Moerner, "Improving the mismatch between light and nanoscale objects with gold bowtie nanoantennas," Phys. Rev. Lett. **94**(1), 017402 (2005).
40. E. C. Le Ru, E. Blackie, M. Meyer, and P. G. Etchegoin, "Surface Enhanced Raman Scattering Enhancement Factors: A Comprehensive Study," J. Phys. Chem. C **111**(37), 13794–13803 (2007).
41. D. P. Fromm, A. Sundaramurthy, A. Kinkhabwala, P. J. Schuck, G. S. Kino, and W. E. Moerner, "Exploring the chemical enhancement for surface-enhanced Raman scattering with Au bowtie nanoantennas," J. Chem. Phys. **124**(6), 061101 (2006).

1. Introduction

Light interaction with nanostructures and nanostructured materials gives rise to various fascinating optical phenomena occurring at the nanoscale [1]. One of the directions of research in nano-optics is the search for structure configurations that efficiently interconvert

propagating and strongly localized optical fields and thereby promote strongly enhanced local fields [2]. The field enhancement (FE) occurs due to the resonantly excited collective electron oscillations [3,4]. Resonant interactions in metal nanostructures involving localized as well as propagating surface plasmons, i.e., surface plasmon-polariton (SPP) modes, have been investigated using colloid metallic nanoparticles (NPs) of various sizes and shapes [5–7], particle ensembles [8] with pre-determined optical properties, and periodic [9,10] and random [11] nanostructures. The spectral position of resonances can be tuned through a variety of parameters such as geometry, composition of nanostructures or size and shape of NPs [12]. These structures or NPs represented well-defined regular configurations exhibiting resonant FE at one or several wavelengths [5–10] or irregular random nanostructures featuring (spatially separated) resonant excitations covering a wide spectrum range [11]. The strong FE is extremely important for practical applications such as sensors [5,7] or micro-optical devices [13] and plays a major role in surface-enhanced Raman scattering (SERS) [9,10,14–16]. SERS is a powerful and highly selective tool to chemically identify and determine the structure of materials and molecules, on the basis of their specific vibrational bonds. Strong SERS effects obtained using nanoplasmonic structures or NPs allows the detection of molecules at extremely low concentrations, down to a single molecule level [17,18]. One way to reach a high FE is to create structures with well-known "hot spots" [18–22]. These so-called hot spots are created at interparticle gaps near 1-3 nm. If gaps turn sub-nanometric, then nonlocal effects start limiting the FE levels [23,24].

There are various strategies for the realization of hot spots, e.g., aggregation of NPs, satellite-systems [25,26], nanostructures fabricated by electron-beam lithography (EBL), and focused ion beam (FIB) milling. However, colloids aggregation is unpredictable random process that leads to alternating Raman enhancement and decreased reproducibility. On the other hand, the EBL and FIB are methods that offer high reproducibility, but these methods are limited to roughly 10 nm gap sizes and require rather costly equipment, thus hindering low-cost and large scale production. After all, the main requirements for SERS substrates are not only high reproducibility and robust fabrication procedure, but also large-area homogeneity, low cost, and possibility for mass production. One route for the fabrication of large-area structures with "hot spots" could be realized with the semi-continuous metallic films [27–29]. These films can be obtained by evaporation of noble metals like gold or silver onto a dielectric or semiconductor substrate. In the beginning of the deposition procedure the "film" consists of separated clusters that grow monotonically in size and with irregular shapes as the amount of deposited gold increases. The clusters tend to grow faster along the substrate plane than in height. As the coverage increases and the deposited gold clusters are beginning to merge together, forming a labyrinthine structure where plasmonic "hot spots" occur for specific thicknesses where the clusters do not form a continuous film, while the distance between clusters is minimal. Using electron-beam deposition it is possible to fabricate structures covering rather large, up to wafer size, areas.

In this work, we experimentally investigate electromagnetic field enhancement effects occurring in thin gold films during their transition from low-coverage (island-like) films, where gold clusters are well separated, to intermediate films near the percolation threshold and, finally, to relatively thick films exhibiting (close to) bulk properties. We anticipate that the results reported in this manuscript will be interesting for applications of various surface-enhanced spectroscopies, in general, and SERS applications (in bio- and molecular sensing and identification), in particular.

2. Fabrication and linear spectroscopy

Thin gold films at different thicknesses were deposited with electron-beam evaporation at a vacuum chamber pressure of 10^{-5} mbar, and a deposition rate of 2 Å/s, onto the room temperature glass (borosilicate) substrates. The films were fabricated with the nominal thicknesses 3, 6, 8, 10, and 12 nm and were subsequently imaged by scanning electron microscopy (SEM) [Fig. 1]. The 3 nm film exhibits separate clusters [Fig. 1(a)], whereas with

increasing thickness until 6 and 8 nm, the clusters form labyrinthine structure [Fig. 1(b) and (c)], and finally almost continuous films for thickness 10 and 12 nm [Fig. 1(d) and (e)].
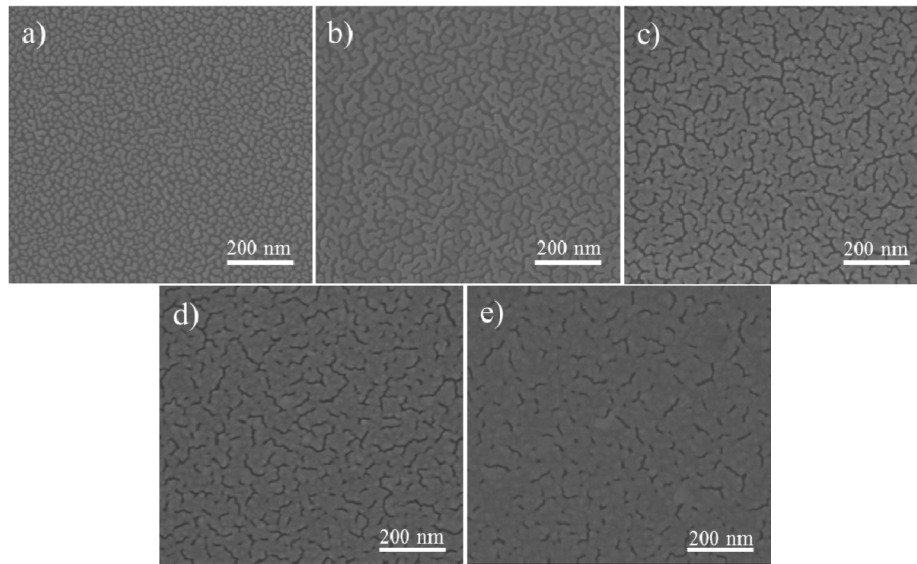

Fig. 1. SEM images of thin Gold films with nominal thicknesses of a) 3nm, b) 6 nm, c) 8 nm, d) 10 nm, and e) 12 nm deposited by electron-beam evaporation on glass substrates.

We emphasize that for the gold films, the quoted "thickness" is the average nominal coverage measured by the quartz oscillator and we estimate variations of the order of $\pm$ 0.5 nm across the wafer. Reflection and transmission spectroscopy [Fig. 2] was performed prior to TPL measurements and before covering the sample with the Raman active dye Crystal Violet (CV). Our experimental setup for reflection and transmission spectroscopy has been described previously [9,10,30]. The spectroscopic reflection and transmission analysis were performed on a BX51 microscope (Olympus) equipped with a halogen light source, polarizers and a fiber-coupled grating spectrometer QE65000 (Ocean Optics) with a wavelength resolution of 1.6 nm. The reflected and transmitted light was collected using an MPlanFL (Olympus) objective with magnification $\times$ 100 (NA = 0.9). The image area analyzed by the spectrometer is limited by a pinhole with a diameter of 150 μm resulting in a circular probing area with a diameter of 1.5 μm. The experimental data in Fig. 2(a) represent the reflection ratio R_{str}/R_{ref}, where R_{str} is the reflection measured from the films and R_{ref} is the reference spectrum recorded from a bulk optically-smooth gold surface. The experimental data in Fig. 2(b) represent the transmission ratio T_{str}/T_{ref}, where T_{str} is the reflection measured from the films and T_{ref} is the reference spectrum recorded from a bare glass substrate. As expected intuitively, the reflectivity of the films increases with nominal thickness, while the transmission decreases [Fig. 2].
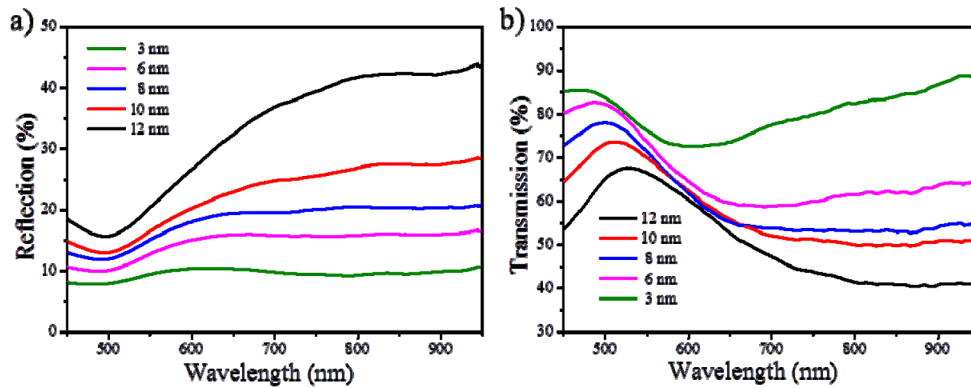
Fig. 2. a) Reflection and b) transmission spectra obtained for the thin gold films with nominal thicknesses of 3 nm, 6 nm, 8 nm, 10 nm, and 12 nm and normalized as explained in the text.

It is seen that, except for the lowest nominal thickness of 3 nm, the spectra do not reveal specific resonances. The reflection spectra resemble those of bulk gold, with the spectral features becoming more pronounced for increasing thicknesses. For the film with thickness 3 nm, the reflection/transmission has a broad peak/dip at ~550-650 nm, which can be explained by local surface plasmon resonances (LSPRs) in clusters with sizes of 10-40 nm [Fig. 1(a)]. At the same time, the peak is inhomogenously broadened, i.e. less pronounced, since the ensemble of clusters have random shapes different heights and orientations.

3. TPL and Raman spectroscopy

Characterization of the FE effects in the fabricated gold films is conducted using TPL [31–33] and Raman microscopy.

3.1 Two photon-excited photoluminescence (TPL) microscopy

The setup consists of a scanning optical microscope in reflection geometry built on the basis of a commercial microscope and a computer-controlled translation stage. The linearly polarized light beam from a mode-locked pulsed (pulse duration ~200 fs, repetition rate ~80 MHz) Ti- Sapphire laser (wavelength $\lambda = 730 – 860$ nm, $\delta\lambda$ ~10 nm, average power ~300 mW) is used as an illumination source at the fundamental harmonic (FH) frequency. After passing an optical isolator (to suppress back-reflection), half-wave plate, polarizer, red color filter and wavelength selective beam splitter, the laser beam is focused on the sample surface at normal incidence with a Mitutoyo infinity-corrected objective ($\times$ 100, N.A. = 0.70). The half-wave plate and polarizer allow accurate adjustment of the incident power. TPL radiation generated in reflection and the reflected FH beam are collected simultaneously with the same objective, separated by the wavelength selective beam splitter, directed through the appropriate filters and detected with two photomultiplier tubes (PMTs). The tube for TPL photons (within the transmission band of 350-550 nm) is connected with a photon counter giving typically only ~20 dark counts per second (cps). The FH and TPL spatial resolution at full-width-half-maximum is ~0.75 μm and ~0.35 μm, respectively, which means no individual clusters will be resolved in the TPL images. In this work, we used the following scan parameters: the integration time (at one point) of 50 ms, scanning speed (between the measurement points) of 20 μm/s, scanned area of 10×10 μm^2, and scanning step size of 350 nm. We adjusted the incident power P within the range 0.3-1 mW in order to obtain significant TPL signals and record the TPL signal dependence on the incident powers. For bulk gold references (both electron-beam deposited and grown single crystalline substrates), we confirmed that obtained TPL signals depend quadratically on the incident power. For these measurements we kept for simplicity the excitation wavelength fixed at 740 nm, since there are no specific resonances Fig. 2 at this wavelength and 740 nm is more visible and

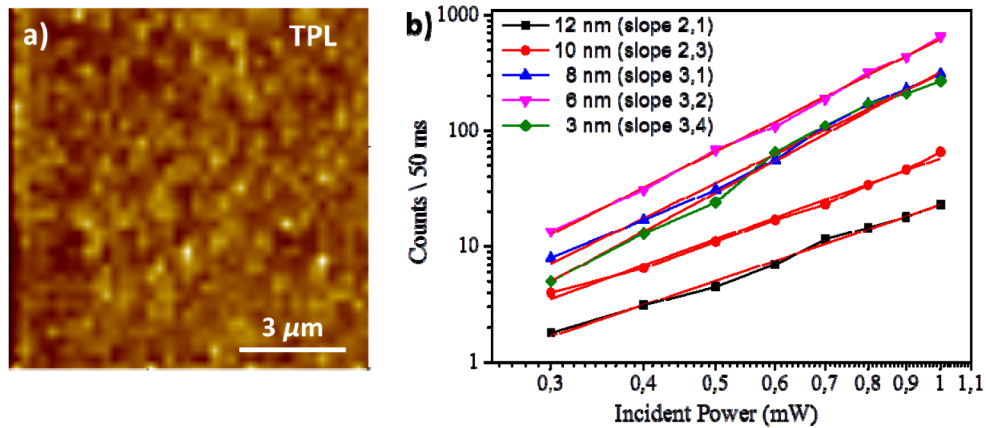convenient to focus. The typical TPL image [Fig. 3(a)] reveals homogeneous signal from the scanned area.

Fig. 3. a) Typical TPL image from the thin gold films, obtained here for 6 nm thickness. (Signal levels at bright spots are typically larger by 30-40% than the average TPL signal). b) Dependence of TPL signal on the power for the thicknesses 3, 6, 8, 10, and 12 nm. The log/log curves are shown with a linear curve fit and slope-values in the legend illustrate the super-cubic signal dependence on incident power.

The TPL measurements show strong TPL signal, which increases with increasing nominal film thicknesses from 3 to 6 nm. For further increase of the film thickness to 8 nm, the TPL signal is again similar to that at 3 nm and dramatically decreases for the thicknesses 10 and 12 nm [Fig. 3(b)]. The remarkable increase of TPL signal can be explained by the coverage approaching the percolation threshold of the gold films. It is important to note that the nominal thickness at which the percolation threshold occurs, depends somewhat on the deposition conditions. We did not perform specific conductivity measurements, which could uniquely indicate the thickness at percolation threshold, but visual analysis of SEM images, clearly indicate that the thickness 3 nm is below, 8-12 nm are above, while 6 nm is in the close vicinity of the percolation threshold [Fig. 1]. It is reasonable that the TPL signal increases for 6 nm thickness as it correlates with the many nano-gaps and -cracks in the film at which hot spots could form [Fig. 1(b)]. With the formation of a continuous film, the number of hot spots significantly reduces and the gold coverage approaches that of a smooth layer [Fig. 1(d) and (e)]. The TPL signal for the 12 nm thickness decreases dramatically compared with that for 6 nm. Meanwhile, the level of TPL signal for the 12 nm film is still above that from the surface of the bulk gold references. The reason is, as was noted above for the thin films, that the film thicknesses is only an average measure. It means that roughness is present not only in the horizontal plane but also in the vertical plane [14,34]. However, we would like to stress that a strongly focused beam will actually also contain z-polarized components, facilitating excitation of longitudinal modes associated with this roughness. The variation of observed TPL signal across the sample was ~15-20% for the thicknesses 3, 6, 8 nm and ~10% for the 10, 12 nm films.

As mentioned above the slope of TPL power dependence should be two, but for some thicknesses [Fig. 3(b)], the TPL-measurements show a non-linear signal with a higher than cubic dependence on incident power. A possible explanation of this higher incident power dependence is supercontinuum white-light generation in the sample [35,36], possibly driven by non-local electron response [37] in the complex geometric shapes of the semi-continues plasmonic nanostructures [38]. It is very important, since it indicates the presence of strong electric fields. Experimentally, the level of TPL enhancement can be objectively evaluated by taking into account the area and incident power producing the TPL signal [39]. The intensity enhancement factor (EF) can be calculated using the following relation:

$$\alpha = \sqrt{\frac{S_{str} \left\langle P_{ref} \right\rangle^2 A_{ref}}{S_{ref} \left\langle P_{str} \right\rangle^2 A_{str}}} \qquad (1)$$

where, S is the obtained TPL signal, $<P>$ is the average incident power, and A is the TPL source area within the FH focus spot (diameter ~0.75 μm) producing the enhancement. Using Eq. (1), the intensity enhancement was estimated for the Gold films as ~14 (12 nm), ~28 (10 nm), ~66 (8 nm), ~96 (6 nm) and ~60 (3 nm). However, these estimations are rather rough as they do not take into account a more detailed ratio between areas, since for the clusters and semi-continues gold it is difficult to accurately evaluate the smaller TPL source area, which would lead to higher FE estimates. Moreover, for such thin films with thicknesses less than the skin depth, not only the source area but also its volume start to play a role, making estimation further complicated. Even if it is possible by a software and SEM images to get an improved estimate of the source area, the film thickness is only an average measure and we cannot be sure of the contributing volume. On the other hand, in the above estimate we did not take into account that the power dependence of the obtained signal is more than quadratic, which would lead to significantly lower FE estimates. The careful calculation for 6 nm thickness with an area reduction, e.g., $A_{str} \sim (40 \times 40 \text{ nm}^2) \sim 1/240 \, A_{ref}$ and accurate power dependence ~3.2, gives the same FE estimation, and it is clear even from these rough estimates that the easily fabricated substrates still provide rather high and interesting FE effects. In the light of Ref [38]. we speculate that the high FE and the nonlinear response could be associated with nonlocal dynamics.

3.2 Surface enhanced Raman spectroscopy

After obtaining the reflection/transmission spectra and TPL characterization, directly before the Raman measurement, the samples were covered by an ethanol 10^{-6} M solution of Crystal Violet dye. This Raman active dye was chosen as it has well characterized properties, and moreover CV is not resonant at our excitation wavelength (absorption line ~590 nm) and it is relatively stable. The non-resonant Raman characterization helps us prevent the strong fluorescence which can sometimes completely dominate the Raman spectra and influence the enhancement estimation. For these experiments the concentration of CV adsorbed at the sample surface is not really important, since we primarily want to combine our understanding of electromagnetic FE with Raman microscopy, using CV dye and the SERS spectral shape for probing of the thin Gold films. The experimental setup used for Raman microscopy is the commercially available confocal scanning Raman microscope (Alpha300R) from Witec and measurements were obtained using linearly polarized excitation of wavelength 532 nm, 600 lines/mm diffraction grating, and × 100 objective (N.A. = 0.90), whereas we use unpolarized detection in order to have a significant signal to noise ratio. Detailed SERS images were formed by mapping the spatial dependence of SERS intensity integrated around the main Raman peaks within the shift range 1560-1650 cm^{-1} for each of the 28 × 28 points (step size 350 nm) in the scan. We used an incident power of P~0.08 mW, and an integration time of 500 ms for each points [Fig. 4(a)].

These scan-parameters were selected as a compromise between minimum damage/bleaching of the dye molecules and significant signal to noise ratios. Typical SERS images show homogeneous signal across the isotropic sample [Fig. 4(a)]. In this connection, we should stress that for all thicknesses, both TPL and SERS images appear very homogenous. Signal levels at bright spots that we observed [Figs. 3(a) and 4(a)] are typically larger by 30-40% than the average TPL signal and by 10-15% than the average SERS signal. We did not observe any *extremely* bright spots, even for thickness close to percolation threshold where the average signal is high.
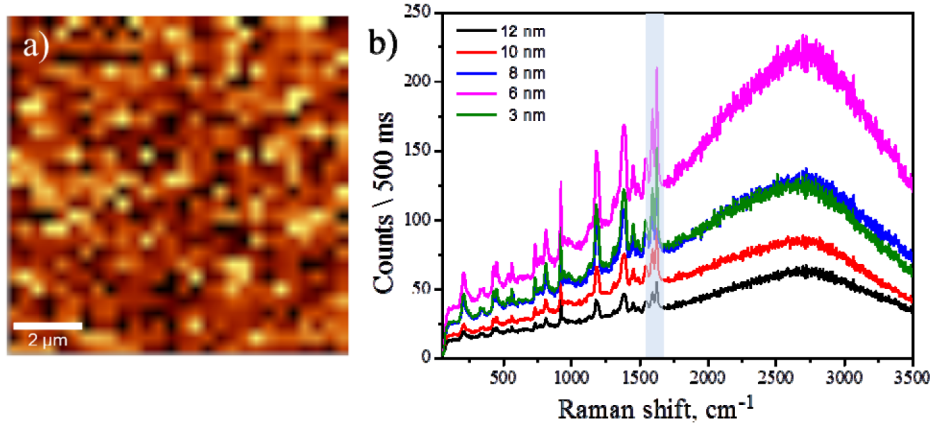
Fig. 4. a) Typical SERS image obtained for the thin Gold films, obtained here for 6 nm thickness. (Signal levels at bright spots larger by 10-15% than the average SERS signal). b) SERS spectra of CV with concentration 10^{-6}M for all thicknesses (3, 6, 8, 10, and 12 nm). The shaded column indicates the range used for SERS imaging in a).

Typical SERS spectra obtained from the thin gold films show that the SERS intensity and fluorescence increases for nominal thicknesses from 3 to 6 nm and then decrease again for 8 nm and continue to decrease for the 10 and 12 nm. Analysis of SEM images explain this behavior as in the case of the 3 nm film thickness [Fig. 1(a)] the gold clusters have sizes ranging from 10 to 40 nm and shapes close to hemi-spheres or elongated rods, with their own LSPRs. The nearest neighbors distance between these clusters is 5-15 nm. The strong SERS originates from LSPRs of these clusters and for this thickness the cluster size and form is important. The increased intensity of the SERS spectra obtained from the film with 6 nm thickness corresponds to increased FE due to a decreased gap between the clusters [Fig. 1(b)]. For this thickness, clusters grow and coalesce into oblong formation of about 20 nm wide and 80-120 nm long. The distance between the nearest neighbors is 15 nm in wide areas and reduces to 1-3 nm in narrow gaps. Some clusters form continuous chains. This happens at a thickness close to percolation threshold and leads to so-called "hot spots" in the nano-gaps between clusters and resulting in an increased SERS signal. With further increasing thickness until 8 nm the size of the clusters increases [Fig. 1(c)], and the amount of "hot spots" decreases. The clusters merge into a labyrinthine structure, hot spots disappear and the roughness of this labyrinthine structure becomes important. For film thicknesses of 10 and 12 nm, the surface looks almost as a homogeneous film. However, since the films with 10 and 12 nm deposition still has some surface roughness, the SERS signal is still present. It should be mentioned that in our previous works we have evaluated the intensity enhancement as the direct ratio between the signal of a reference (obtained signal form the smooth bulk gold film) and the main Raman peaks from dye adsorbed on the structures [9,10]. In the present case, we could not use this method since, with the dye deposited at the same concentration, it was not possible to get a Raman signal on smooth gold. For the calculation of enhancement, we use the analytical EF expression which quantifies how much more signal can be expected from SERS in comparison with normal Raman for the same experimental parameters [40]. The average EF was determined by comparing the signals acquired from CV at a concentration of 5×10^{-2} M on a glass substrate, with the signals obtained from 10^{-6} M of CV on the thin gold films. The EF was calculated using the following relation:

$$EF = \frac{I_{SERS}}{I_{ref}} \frac{C_{ref}}{C_{SERS}},$$

(2)

where I_{SERS} and I_{ref} represent background-subtracted intensities of the 1626 cm^{-1} band (being the most intense band) for CV adsorbed on the thin gold films and on the glass substrate,

respectively. C_{SERS} and C_{ref} represent the corresponding concentrations of CV on these different substrates. The average EF of these thin gold films were estimated to be ~0.85×10^4 (3 nm), ~1.07×10^4 (6 nm), ~0.63×10^4 (8 nm), ~0.45×10^4 (10 nm), and ~0.25×10^4 (12 nm), respectively. We would like to stress that in this case that we have used non-resonant dye at the excitation wavelength, whereas for the resonant case the enhancement estimation would be one or two order of magnitude higher. In addition, although the investigated semi-continuous gold films do not provide as strong enhancements factors as reported for other specifically prepared gold structure configuration [5], our surfaces qualify as intermediate simple and large-scale fabricated SERS substrates. At the 532 nm excitation wavelength used for SERS imaging, the SPPs have considerably shorter propagation lengths of only a few micrometers, but at the same time this excitation wavelength is close to the LSPR of the individual clusters. Furthermore, one should note that in addition to the different excitation wavelengths there is also a fundamental difference between using TPL and SERS for the FE estimation. Here, TPL originates from the gold structure itself (contribution from the bulk), whereas SERS is from the part of analyte located close to the surface with strong fields and near or in hot spots, and in addition, there is a chemical enhancement [41], present due to chemical interactions between analyte and the gold film itself.

4. Summary

In conclusion, we have investigated the scattering properties and the local FE of 3, 6, 8, 10, 12 nm thin gold films using reflection and transmission spectroscopy, nonlinear two-photon photoluminescence scanning optical microscopy, and Raman microscopy. The reflectivity of the semi-continuous films increases with nominal thickness, while the transmission decreases. The extremely strong and homogeneous TPL-signal was observed across the sample close to the percolation threshold, for a thickness of 6 nm, and a decreasing signal for further increasing nominal thickness. For thicknesses of 3, 6 and 8 nm, the TPL-measurement shows a non-linear signal with a higher than cubic dependence on incident power, rather than the quadratic dependence expected from regular TPL-measurements. Such strong power dependence could be related to super-continuum white-light generation involving various high-order nonlinear processes and it is an important signature of strong FE. For the Raman measurements, the samples were covered with 10^{-6} M concentration of Crystal Violet dye, which is non-resonant at the excitation wavelength of 532 nm. The SERS thickness dependence follows a similar trend as observed for the TPL investigation, with an increasing Raman signal for the 6 nm thickness, indicating how SERS enhancement is promoted near the percolation threshold. We believe that these easy-to-fabricate and scalable semi-continuous metallic films constitute a practical alternative for designing SERS substrates to be employed in the single-molecule detection and that the possibility for supercontinuum white-light generation in the percolation geometry should be investigated further, using also spectral and time-resolved measurements.

Acknowledgments